Journal of Hazardous Materials 371 (2019) 1–7

Contents lists available at ScienceDirect

Journal of Hazardous Materials

journal homepage: www.elsevier.com/locate/jhazmat

# Explosion characteristics for Li-ion battery electrolytes at elevated temperatures

M. Henriksen[a,*], K. Vaagsaether[a], J. Lundberg[a], S. Forseth[b], D. Bjerketvedt[a]

[a] Faculty of Technology, Natural Sciences and Maritime Sciences, University of South-Eastern Norway, Kjølnes Ring 56, Porsgrunn, 3901, Norway
[b] Norwegian Defence Research Establishment (FFI), Instituttveien 20, 2007, Kjeller, Norway

ARTICLE INFO

*Keywords:*
Dimethyl carbonate
Diethyl carbonate
Ethyl methyl carbonate
Maximum explosion pressure
The maximum rate of explosion pressure rise

ABSTRACT

Li-ion batteries are used in electronic devices and electric cars, yet they create safety concerns due to the possibility of the release of combustible materials. The electrolyte, one of the main components in a Li-ion cell, consists of organic carbonates. Venting and thermal runaway release organic carbonates and when mixed with air, it can result in fires and explosions. A 20-liter explosion sphere was used to determine the explosion characteristics for three typical carbonates used in electrolytes, at 373 K, and 100 kPa absolute pressure. The explosion pressure and the maximum rate of explosion pressure rise are presented for the carbonates and for hydrogen, methane, and propane, and the explosive limits for the carbonates are also identified at the same conditions. This allowed a comparison of the explosion characteristics for the carbonates with those for hydrogen, methane, and propane. Theoretical calculations gave a higher explosion pressure than that from the experimental results most likely due to losses in the hydrocarbon experiments. The carbonates analyzed have very similar explosion pressures and rate of explosion pressure rise as propane. The explosion characteristics found for the three carbonates can be used in future consequence and risk assessments for Li-ion battery installations.

## 1. Introduction

A wide range of products uses Li-ion batteries, from cellular phones and computers to hybrid, fuel cell, and electric vehicles. A high energy density, low self-discharge, and low maintenance are advantages that distinguish Li-ion batteries from traditional batteries [1]. One of the main components of a Li-ion battery/cell is the electrolyte. The electrolyte consists of one or a mixture of organic carbonates together with a Li-ion salt, i.e., $LiPF_6$. The flammable electrolyte is a potential hazard [2,3] and in the last two decades, there have been several reports of fire and explosion related incidents caused by Li-ion battery failure [4]. Li-ion battery failure can be caused by several different events, such as mechanical abuse, overcharge, heat exposure, over-discharge, external and internal short-circuit [5]. Battery failure can lead to the release of a combustible mixture and under certain conditions, thermal runaway can occur [6–8]. The combustible mixture that is release can consist of organic carbonates and other combustible gases such as hydrogen, methane, and propane in addition to particulate matter [5,9]. It is this release of combustible materials mixed with air that can cause fires and explosions [4–6,9–11]. Fig. 1 shows two still images of an inhomogeneous propagating flame caused by from the released gas/mist vented from an externally heated 18,650 Li-ion cell.

Explosion characteristics such as the explosion pressure, the rate of explosion pressure rise, and upper and lower explosive limits (UEL and LEL, respectively) are critical parameters for consequence and risk assessment [12–14]. Explosion pressure and the rate of explosion pressure rise are also used to verify computational models. Essential explosion characteristic data for dimethyl carbonate (DMC), ethyl methyl carbonate (EMC), and diethyl carbonate (DEC) are missing in the literature. Only the explosive limits for DMC and DEC have been reported but without a description of the experimental conditions [15,16].

In this study, the explosion characteristics for DMC, EMC, and DEC were analyzed in a 20-liter explosion sphere. The initial conditions for all experiments were 100 kPa absolute and 373 K. Hydrogen, methane, and propane are also analyzed and compared with previously published results [17–22].

## 2. Materials and method

The vessel used in the experiments was a standard 20-liter Anko explosion sphere, which is in accordance with standards EN-1839 [23] and EN-13673-1 [24]. Fig. 2 shows a photo and a schematic drawing of

* Corresponding author at: University of South-Eastern Norway, PEM, Kjølnes Ring 56, Porsgrunn, 3901, Norway.
*E-mail address:* mathias.henriksen@usn.no (M. Henriksen).

https://doi.org/10.1016/j.jhazmat.2019.02.108
Received 12 April 2018; Received in revised form 26 February 2019; Accepted 27 February 2019
Available online 28 February 2019
0304-3894/ 

**Nomenclature**

*Variables/Parameters*

| | |
|---|---|
| $P_{ex}$ | Maximum explosion pressure from experiment |
| $P_{max}$ | Maximum explosion pressure from a series of experiments |
| $(dp/dt)_{ex}$ | Maximum rate of explosion pressure rise from an experiment |
| $(dp/dt)_{max}$ | Maximum rate of explosion pressure rise from a series of experiments |
| $K_G$ | Deflagration index for an experiment |
| LEL | Lower explosive limit |
| UEL | Upper explosive limit |
| $\phi$ | Fuel-air equivalence ratio |

the explosion sphere used. Two Kistler 601CAA pressure transducers measured the explosion pressure at 100 kHz. A Keller PAA-33X pressure transducer recorded the pressure during the filling process to get the partial pressures for each component. Separate injection ports for all materials were used to reduce uncertainties in the fuel-air concentration. There were two types of ignition systems used. The wire ignition system, used to determine LEL and UEL, causes a metal wire to melt and evaporate, which then ignites the mixture. The ignition energy is approximately 10 J according to the supplier. The spark ignition system was used to achieve the explosion pressure ($P_{ex}$) and the maximum rate of explosion pressure rise ($(dp/dt)_{ex}$). The spark ignition is a series of electrical sparks between two electrodes that has a total duration of 0.5 s. The temperature set point for the apparatus was chosen to be 373 K instead of the typical value of 298 K due to a relatively low vapor pressure for DEC at 298 K A Photron high-speed camera recorded each experiment that was conducted with the spark ignition for visual in-

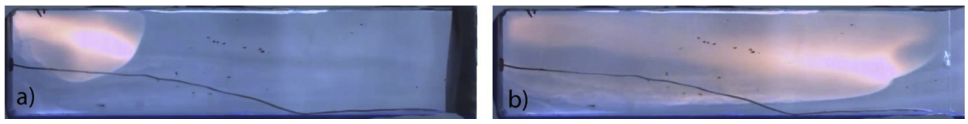


**Fig. 1.** Two still images of an inhomogeneous flame propagating inside a 0.45 × 0.10 × 0.10 explosion channel. A 18650 Li-ion cell was externally heated until the combustible gas/mist vented. a) Short after the ignition. b) Image when the flame has reached the end of the channel.

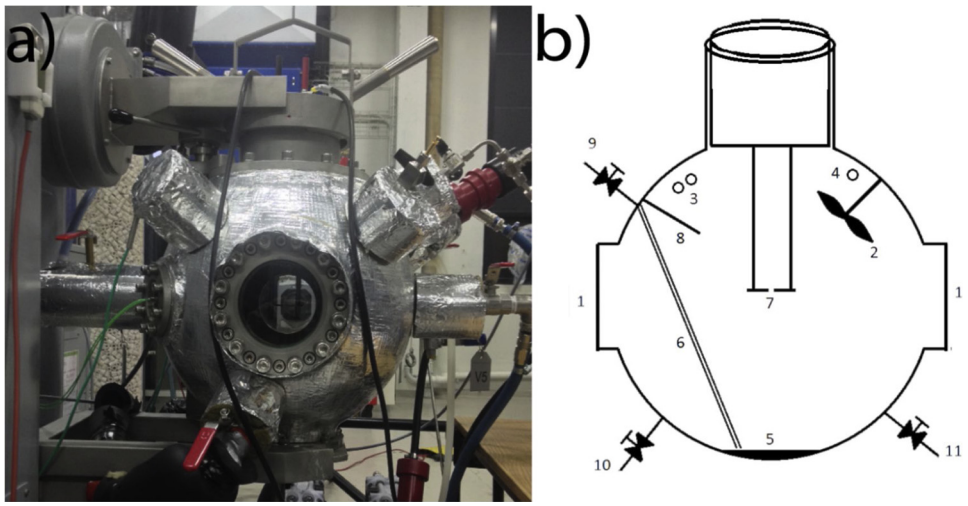


**Fig. 2.** (a) Photo of the 20-liter explosion sphere. (b) Illustration of the 20-liter explosion sphere. 1: 0.1 m windows; 2: mixing propeller; 3: Kistler pressure transducers; 4: Keller pressure transducer; 5: liquid evaporator; 6: liquid sample tube; 7: spark igniter; 8: ambient temperature probe; 9: liquid injection port; 10: fuel (gas) injection port; 11: air injection port.

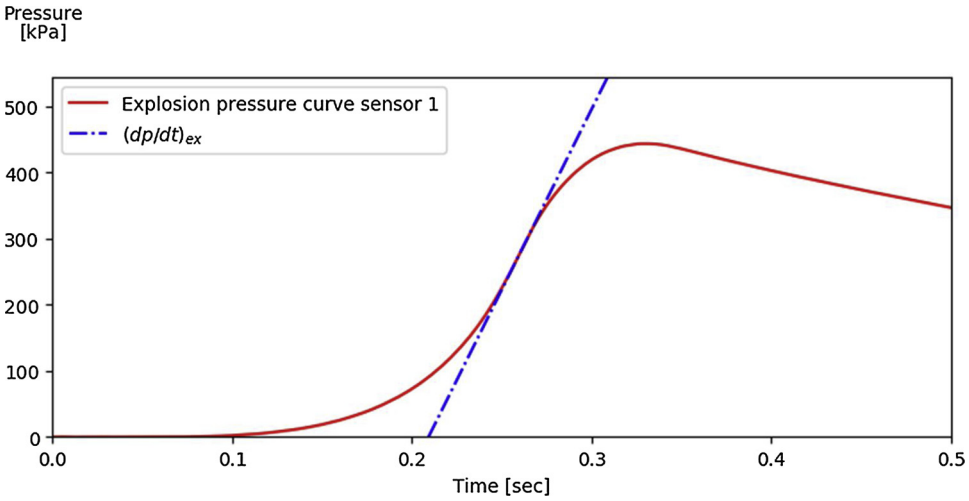


**Fig. 3.** The filtered explosion pressure measurement, with the calculated $(dp/dt)_{ex}$ line, for the 4.2% dimethyl carbonate experiment. This plot was used to validate the linear regression of the rate of explosion pressure rise.

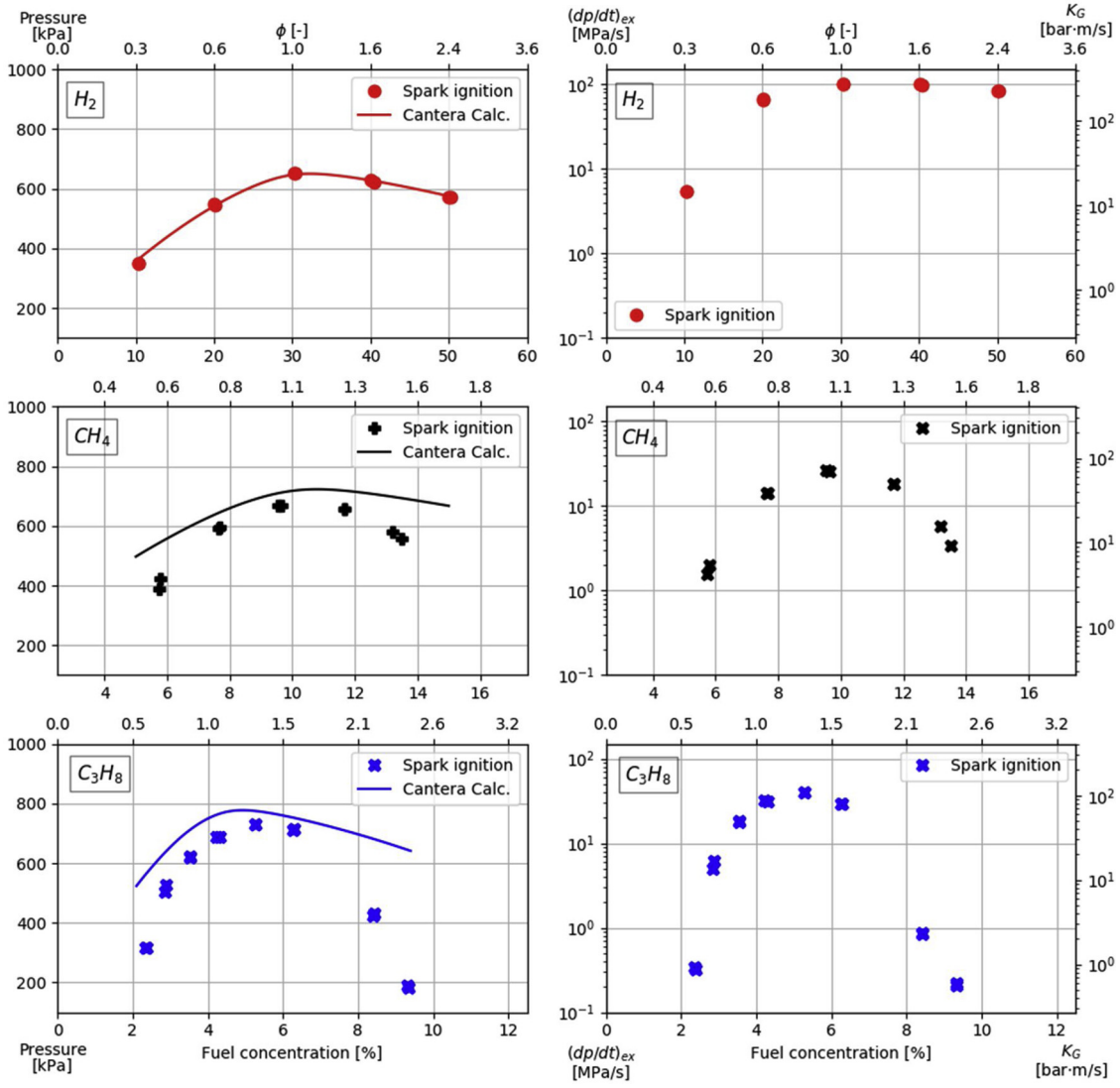


**Fig. 4.** Left: The maximum explosion pressure ($P_{ex}$) from each experiment. Right: The maximum rate of explosion pressure rise ($(dp/dt)_{ex}$) from each experiment. The initial absolute pressure and temperature was 100 kPa and 373 K, respectively.

**Table 1**
Summary of the primary results from the hydrogen, methane, and propane experiments at 373 K and 100 kPa.

| Variables/Parameters | Materials | | | | | |
|---|---|---|---|---|---|---|
| | Hydrogen | | Methane | | Propane | |
| $P_{ex}$ ($\phi \approx 1$) | $\phi$ = 1.04 | 653 kPa | $\phi$ = 1.00 | 670 kPa | $\phi$ = 1.05 | 687 kPa |
| $P_{max}$ | $\phi$ = 1.04 | 653 kPa | $\phi$ = 1.02 | 670 kPa | $\phi$ = 1.32 | 729 kPa |
| $(dp/dt)_{max}$ | $\phi$ = 1.04 | 101.9 MPa/s | $\phi$ = 1.02 | 26.8 MPa/s | $\phi$ = 1.32 | 40.6 MPa/s |
| $K_{G,max}$ | 276.6 (bar·m)/s | | 72.7 (bar·m)/s | | 110.3 (bar·m)/s | |

spection.

The explosion sphere was purged with compressed and oil-free air for a minimum of five minutes, exchange the total volume in the sphere approximately 40 times, before each experiment. The explosion sphere was evacuated to an absolute pressure of 10 kPa or less, after purging. Fuel was filled to the desired partial pressure, and then the sphere was filled with air to 100 kPa ( ± 0.5 kPa). Air and fuel were actively mixed for three and a half minutes to ensure a homogenous mixture. After mixing, the temperature was recorded. The temperature difference between experiments was within ± 2.5 K. The ignition was delayed for one and a half minutes after mixing to ensure that the mixture was quiescent. For $P_{ex}$ and $(dp/dt)_{ex}$, two parallel experiments were conducted for each target concentration. Five parallel experiments with no ignition were performed to determine the explosive limits.

Alfa Aesar was the supplier for EMC and Sigma-Aldrich the supplier for DMC and DEC. All three carbonate solutions had 99% purity or higher and bought from Sigma Aldrich Norway. AGA Linde Norway supplied the hydrogen, methane, and propane with a purity of 99.95% or higher.

The explosion pressure measurement was post-filtered with a Savitzky-Golay smoothing algorithm [25]. All experiments had identical smoothing-filter parameters at 999 data points and a second-order polynomial fit. For each experiment, the average maximum pressure for the two filtered data sets determined $P_{ex}$. The algorithm below was used

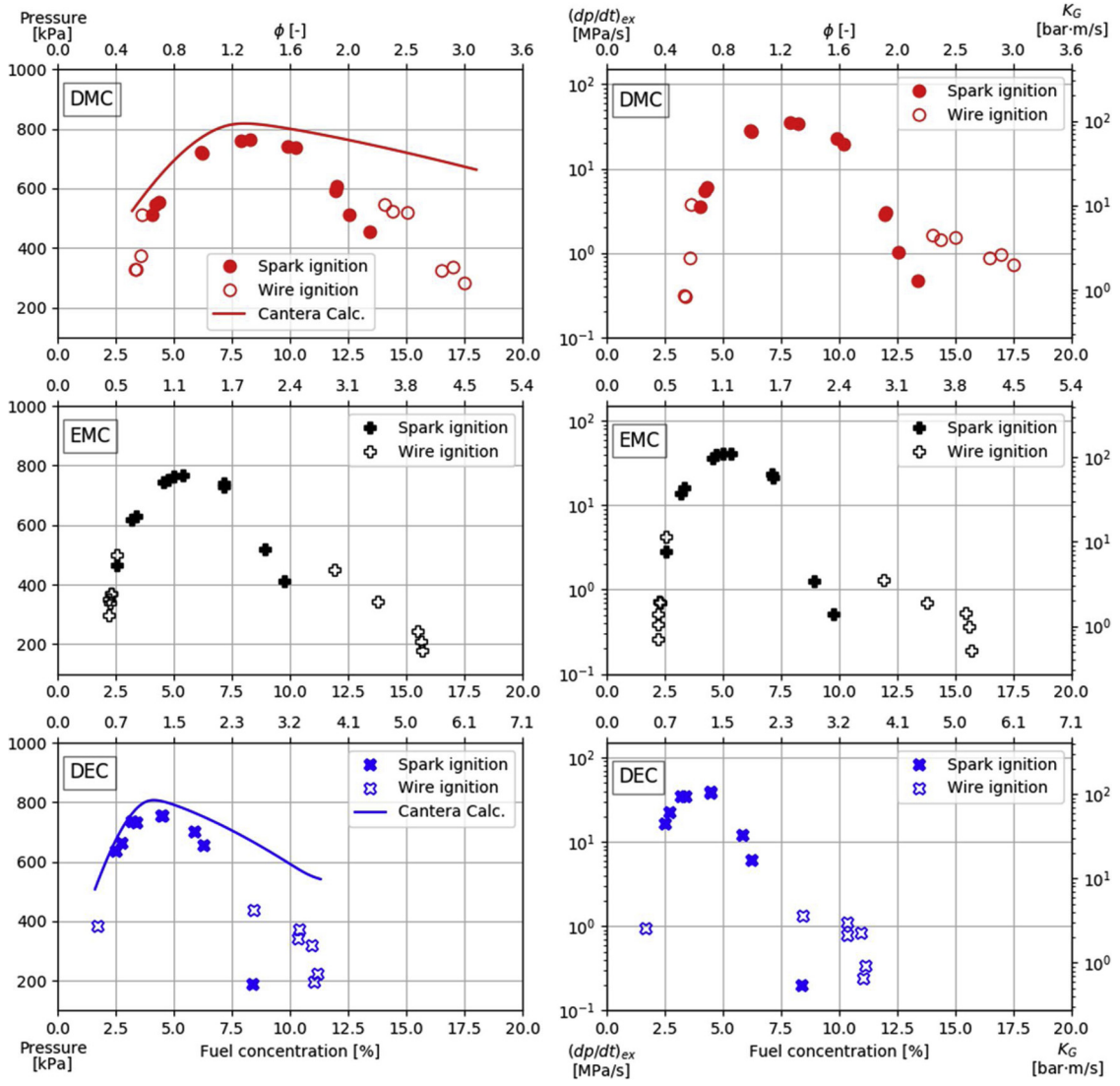


**Fig. 5.** Left: The maximum explosion pressure ($P_{ex}$) from each experiment. Right: The maximum rate of explosion pressure rise ($(dp/dt)_{ex}$) from each experiment. The initial absolute pressure and temperature was 100 kPa and 373 K, respectively.

**Table 2**
Summary of the primary results from the dimethyl carbonate (DMC), ethyl methyl carbonate (EMC), and diethyl carbonate (DEC) experiments with initial conditions at 373 K and 100 kPa.

| Variables/Parameters | Materials | | | | | |
|---|---|---|---|---|---|---|
| | DMC | | EMC | | DEC | |
| $P_{ex}$ ($\phi \approx 1$) | $\phi = 0.95$ | 720 kPa | $\phi = 1.02$ | 744 kPa | $\phi = 1.00$ | 731 kPa |
| $P_{max}$ | $\phi = 1.28$ | 763 kPa | $\phi = 1.22$ | 768 kPa | $\phi = 1.34$ | 757 kPa |
| $(dp/dt)_{max}$ | $\phi = 1.23$ | 34.8 MPa/s | $\phi = 1.13$ | 41.4 MPa/s | $\phi = 1.33$ | 38.9 MPa/s |
| $K_{G,max}$ | 94.5 bar m/s | | 112.4 bar m/s | | 105.7 bar m/s | |
| LEL | 3.2% | | 2.1% | | 1.6% | |
| UEL | 18.0% | | 15.8% | | 11.3% | |

to calculate $(dp/dt)_{ex}$:

- Find gradients in the filtered pressure data
- Filter gradient data to remove noise
- Use the largest gradient as the starting point for the $(dp/dt)_{ex}$ calculation
- Conduct a 150-data-point regression to find the maximum gradient, $(dp/dt)_{ex}$

Fig. 3 shows one of the control images produced to validate the $(dp/dt)_{ex}$ algorithm. The highest maximum rate of explosion pressure rise for a series of experiments ($(dp/dt)_{max}$) was used to calculate the deflagration index ($K_G$) for one material. Eq. (1) is used to calculate the deflagration index. The standard unit for $K_G$ is (bar·m)/s, which was therefore used in this study.

$$K_G = \left(\frac{dp}{dt}\right)_{max} \cdot V^{\frac{1}{3}} \quad (1)$$

where $K_G$ is the deflagration index for gases [(bar·m)/s], $(dp/dt)_{max}$ is the maximum rate explosion pressure rise from a series of experiments [bar/s], and $V$ is the volume of the explosion sphere [$m^3$].

The chemical kinetics, thermodynamics, and transport process simulation tool Cantera (version 2.3.0) [26] was used to calculate $P_{ex}$ theoretically. To calculate the $P_{ex}$, the standard equilibrium solver was used with constant internal energy, constant volume, and the same initial conditions as in the experiments. This theoretical calculation was also referred to as closed volume combustion or adiabatic isochoric complete combustion (AICC). The reaction mechanism for DMC was taken from Glaude et al. [27]; that for DEC was from Nakamura et al. [28]; and the Gri3.0 reaction mechanism for hydrogen, methane, and propane was from Smith et al. [29]. The established reaction mechanism for the different fuels provided the equilibrium constants and reaction sets for the calculation. No reaction mechanism for EMC was found and thus no theoretical calculation of explosion pressure.

## 3. Results

Fig. 4 shows the experimental results for hydrogen, methane, and propane with the $P_{ex}$ on the left and $(dp/dt)_{ex}$ on the right. Propane had the highest maximum explosion pressure ($P_{max}$) at 729 kPa, and hydrogen had the highest $(dp/dt)_{max}$ at 101.9 MPa/s. Of the three fuels, hydrogen had the smallest discrepancy between the experimental results and the theoretical calculations. For methane and propane, the disagreement between these results was approximately 40 kPa for a fuel-air equivalence ratio ($\phi$) between 0.75 and 1.5. The average difference between all parallels was 3 kPa for the three fuels. Table 1 summarizes the primary results in Fig. 4.

Fig. 5 shows the results from the DMC, EMC, and DEC experiments. EMC has the highest $P_{max}$ and $(dp/dt)_{max}$, at 768 kPa and 41.4 MPa/s, respectively. DMC and EMC have a slightly lower $P_{max}$, with the small difference of 11 kPa. There is disagreement in $P_{ex}$ between the experimental and theoretical results for both DMC and DEC. For $0.65 \leq \phi \geq 1.6$, the discrepancy is approximately 50 kPa. For $\phi > 1.6$, the gap between the results and calculations increases significantly. The average difference between parallels for all experiments and all three fuels was calculated to be 8 kPa.

The open symbols in Fig. 5 show the experiments where ignition occurred when iterating toward the explosive limits. The explosive limits for both DMC [15] and DEC [16] were found on the International Programme on Chemical Safety (IPCS) INCHEM database. Table 2 summarizes the results from the experiments with DMC, EMC, and DEC. Table 3 summarizes the calculated pressures and explosive limits found in literature.

## 4. Discussion

To validate the procedure and experimental setup and to quantify the variation between experiments, two parallel experiments were performed at each target concentration. A comparison of the spark ignition experiments (solid symbols) in Figs. 4 and 5 show that there is only a small difference in $P_{ex}$ and $(dp/dt)_{ex}$ for two parallels. DMC, EMC, and DEC have greater differences in $P_{ex}$ than hydrogen, methane, and propane: 8 kPa and 3 kPa, respectively. This difference is likely caused by the variation in concentration for the two liquid parallels. The syringe used to inject the liquid made it hard to obtain an exact concentration for each parallel. The experimental results were also compared with a theoretical calculation performed using Cantera. Figs. 4 and 5 and Tables 2 and 3 show that there is a discrepancy between the results and calculations in all cases except for hydrogen. The difference is within 50 kPa for $0.65 \leq \phi \leq 1.6$. For methane and propane, the disagreement between the theoretical calculation and experiments is in the same range as previously published results [18,19,21]. The experimental results for hydrogen, methane, and propane at 298 K and 373 K was in good agreement with previously published experimental results at similar conditions [17–22]. Spark ignition was chosen for the $P_{ex}$ and $(dp/dt)_{ex}$ experiments since it resulted in a lower variation between two parallels: 0.44 MPa/s, and 1.38 MPa/s, respectively. The procedure and experimental setup provided reproducible results with little variation between parallels.

The differences between the theoretical and experimental results are most likely due to heat loss in the experiments. Since the calculations are adiabatic and reach chemical equilibrium, they are ideal with no losses. The experimental setups have radiative heat loss, especially for the hydrocarbon materials. Bradly [30] estimated a heat loss of 5% for spherically shaped combustion with a radius of 0.5 m in methane and propane experiments. The radiative heat loss for hydrogen is less than that for hydrocarbons. Since hydrogen has a low radiative flux and high $(dp/dt)_{ex}$ (short combustion time), the experimental results are very close to the theoretical results. For $\phi$ above 1.6, the disagreement between calculation and experiments increases for hydrocarbons, as shown in Figs. 4 and 5. The discrepancy is not only due to heat losses from radiation, but also due to other effects, as buoyancy causing a non-spherical flame and soot formation. Dahoe [31] reported that buoyancy would have a more significant effect on the experiments when concentrations approached the explosive limits. The flame front would be mushroom shaped instead of spherical. Heat loss would then occur in the upper part of the vessel due to the direct contact between the combustion products and the walls before the flame reaches the lower walls. Heat loss at the top from convection will influences the explosion pressure. The high-speed video for mixtures close to the explosive limits clearly shows a mushroom-shaped flame front. At rich conditions, soot also forms for hydrocarbons. Soot residue was found inside the explosion sphere for experiments that were close to the explosive limits for most of the hydrocarbon experiments. None of the reaction mechanisms used in the theoretical calculations included the formation or reaction of soot. The radiative heat loss will also increase due to the high radiative properties of soot and increased combustion time.

The three carbonates have very similar $P_{ex}$ and $(dp/dt)_{ex}$. Only 11 kPa separates the highest and lowest $P_{max}$, which is close to the variation between parallels at 8 kPa. The difference of 6.6 MPa/s in $(dp/dt)_{max}$ is regarded as relatively small and will only give a minimal difference in vent areas [12,13]. Since the results from all three carbonates are within the same range, the preliminary risk assessment is simplified. In the course of a thermal runaway, carbonates will decompose into other materials, such as hydrogen, carbon monoxide, carbon dioxide, and ethylene, among others. The composition of the vented gas is dependent on the state of charge (SOC) and electrolyte mixture [5,7,9,32]. The explosion characteristics for this gas mixture may differ from the results of this study. Further study in dispersion rates, vented material concentration, and total vented mass from known Li-ion cell compositions are needed to improve the consequence and risk assessment of Li-ion batteries further.

DMC showed the most significant discrepancy in LEL and UEL compared with previous data [15]. The absolute difference is -1% for LEL and +5.1% for UEL when comparing the results in Table 2 and the literature values in Table 3. In the IPCS safety chemical database for DMC, the temperature and pressure for the explosive limits are not

**Table 3**
Theoretical calculation of the maximum explosion pressure and the literature values for the lower and upper explosive limit for dimethyl carbonate and diethyl carbonate.

| Variables/Parameters | Materials | | | |
|---|---|---|---|---|
| | DMC | | DEC | |
| $P_{ex}$ ($\phi$ = 1, theoretical) | $\phi$ = 1.00 | 788 kPa | $\phi$ = 1.00 | 778 kPa |
| $P_{max}$ (theoretical) | $\phi$ = 1.25 | 818 kPa | $\phi$ = 1.23 | 807 kPa |
| LEL [15,16] | 4.22% | | 1.4% | |
| UEL [15,16] | 12.87% | | 11.0% | |

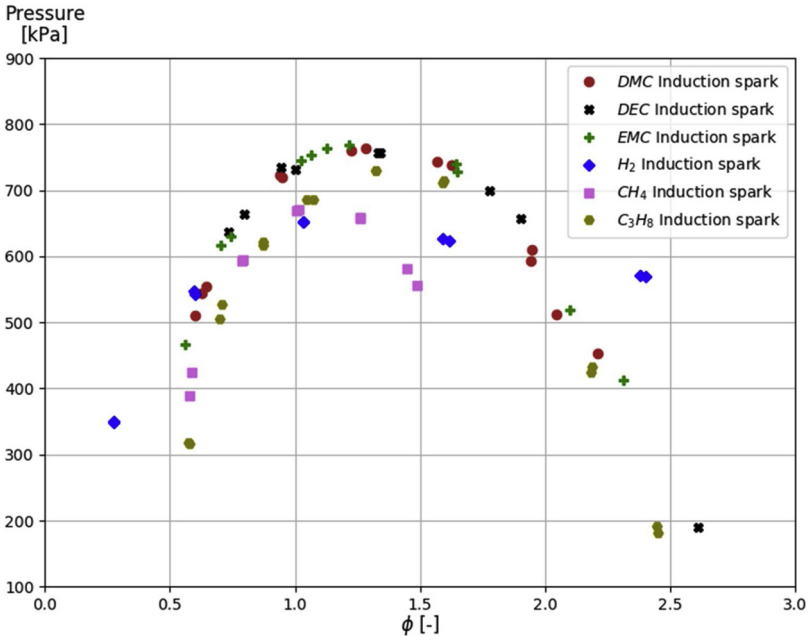


**Fig. 6.** Explosion pressure for all experiments. The initial absolute pressure and temperature were 100 kPa and 373 K, respectively.

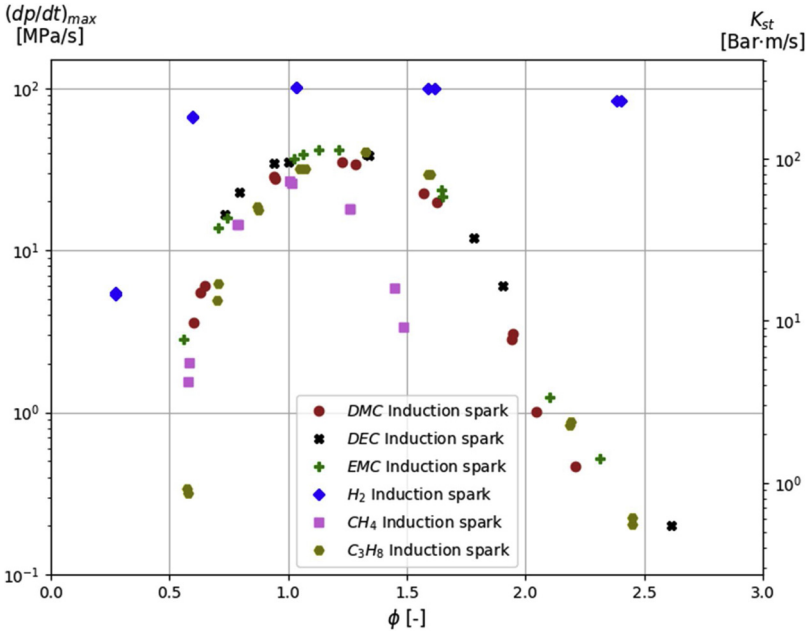


**Fig. 7.** The rate of explosion pressure rise for all experiments. The initial absolute pressure and temperature were 100 kPa and 373 K, respectively.

reported. The initial conditions for the explosive limits may differ from the 373 K and 100 kPa conditions used in this study. This may be the cause of the relatively large gap in explosive limits. The difference in explosive limits in this study and the IPSC database [16] was less for DEC than for DMC. The small discrepancy between reported explosive limits is not unexpected if there were differences in the experimental setups [17].

Figs. 6 and 7 compare $P_{ex}$ and $(dp/dt)_{ex}$ for all experiments with spark ignition. Fig. 6 shows that there is little difference in the $P_{ex}$ for the carbonate experiments. Hydrogen and methane have a lower $P_{ex}$ compared with the carbonates. Propane has a very similar $P_{ex}$ and $(dp/dt)_{ex}$ profile as the carbonates. Fig. 7 shows that, of all experiments, hydrogen has the highest $(dp/dt)_{ex}$. Considering hydrogen's high laminar burning velocity relative to the other materials, this is expected [10]. Since all the experiments are performed in the same explosion vessel volume, the $(dp/dt)_{max}$ and $K_G$ are linearly related. Therefore, $K_G$ is not discussed any further. The explosion characteristics of a Li-ion electrolyte (a different mixture of carbonates) are comparable to the explosion characteristics of propane. When estimating the consequence for Li-ion batteries with an unknown electrolyte, it may be useful to assume propane explosion characteristics initially.

## 5. Conclusion

A 20-liter explosion sphere was used to determine the explosion pressure, the rate of explosion pressure rise, and the lower and upper explosive limit for dimethyl carbonate, diethyl carbonate, and ethyl methyl carbonate at different concentrations, with the initial condition at 373 K and 100 kPa. The procedure and experimental setup gave reproducible results and is considered a suitable method for determining

explosion characteristics. All three carbonates have similar explosion pressure and rate of explosion pressure rise.

An adiabatic and chemical equilibrium calculation performed using Cantera gave higher explosion pressures compared to experiments for all materials expect hydrogen. This disagreement is reported in other publications and is typical for hydrocarbons [18,19,21]. The difference in explosion pressure between the theoretical calculation and experiments increases for a fuel-air equivalence ratio above 1.7, due to heat loss, non-spherical-shaped combustion, and soot formation.

The explosion characteristics for the three carbonates were compared to experiments with hydrogen, methane, and propane. Propane has very similar explosion characteristics as the carbonates. The results obtained from the experiments with the three carbonates are considered novel and can be of use in future consequence and risk assessments for Li-ion battery installations.

## Acknowledgments

This work was performed within MoZEES, a Norwegian Centre for Environment-friendly Energy Research (FME), co-sponsored by the Research Council of Norway (project number 257653) and 40 partners from research, industry and public sector.

## References

[1] Battery University, What's the Best Battery? Battery Univ., 2017, http://batteryuniversity.com/learn/archive/whats_the_best_battery.
[2] S.J. Harris, A. Timmons, W.J. Pitz, A combustion chemistry analysis of carbonate solvents used in Li-ion batteries, J. Power Sources 193 (2009) 855–858, https://doi.org/10.1016/j.jpowsour.2009.04.030.
[3] S. Hess, M. Wohlfahrt-Mehrens, M. Wachtler, Flammability of Li-Ion battery electrolytes: flash point and self-extinguishing time measurements, J. Electrochem. Soc. 162 (2015) A3084–A3097, https://doi.org/10.1149/2.0121502jes.
[4] D. Lisbona, T. Snee, A review of hazards associated with primary lithium and lithium-ion batteries, Process Saf. Environ. Prot. 89 (2011) 434–442, https://doi.org/10.1016/j.psep.2011.06.022.
[5] C.C. Crafts, D.H. Doughty, J. McBreen, E.P. Roth, Advanced Technology Development Program for Lithium-ion Batteries : Thermal Abuse Performance of 18650 Li-ion Cells, (2004), https://doi.org/10.2172/918751.
[6] Q. Wang, P. Ping, X. Zhao, G. Chu, J. Sun, C. Chen, Thermal runaway caused fire and explosion of lithium ion battery, J. Power Sources 208 (2012) 210–224, https://doi.org/10.1016/j.jpowsour.2012.02.038.
[7] B. Lei, W. Zhao, C. Ziebert, N. Uhlmann, M. Rohde, H. Seifert, Experimental analysis of thermal runaway in 18650 cylindrical Li-Ion cells using an accelerating rate calorimeter, Batteries 3 (2017) 14, https://doi.org/10.3390/batteries3020014.
[8] F. Jiang, K. Liu, Z. Wang, X. Tong, L. Guo, Theoretical analysis of lithium-ion battery failure characteristics under different states of charge, Fire Mater. 42 (2018) 680–686, https://doi.org/10.1002/fam.2522.
[9] P. Ribière, S. Grugeon, M. Morcrette, S. Boyanov, S. Laruelle, G. Marlair, Investigation on the fire-induced hazards of Li-ion battery cells by fire calorimetry, Synth. Lect. Energy Environ. Technol. Sci. Soc. 5 (2012) 5271–5280, https://doi.org/10.1039/C1EE02218K.
[10] J. Johnsplass, M. Henriksen, K. Vaagsaether, J. Lundberg, D. Bjerketvedt, Simulation of Burning Velocities in Gases Vented From Thermal run-a-way Lithium Ion Batteries, (2017), pp. 157–161, https://doi.org/10.3384/ecp17138157.
[11] C. Mikolajczak, M. Kahn, K. White, R.T. Long, Lithium-Ion Batteries Hazard and Use Assessment, Springer US, Boston, MA, 2011, https://doi.org/10.1007/978-1-4614-3486-3.
[12] D.A. Crowl, J.F. Louvar, Chemical Process Safety: Fundamentals With Applications, 2nd ed., Prentice Hall PTR, Upper Saddle River, N.J, 2002.
[13] F.P. Lees, Loss Prevention in the Process Industries: Hazard Identification, Assessment and Control, 2. Ed., Butterworth-Heinemann, Oxford, 1996.
[14] D. Bjerketvedt, J.R. Bakke, K. Van Wingerden, Gas explosion handbook, J. Hazard. Mater. 52 (1997) 1–150.
[15] IPCS INCHEM, Dimethyl carbonate, Int. Programme Chem. Saf. INCHEM, (2005) (Accessed 21 December 2018), http://www.inchem.org/documents/icsc/icsc/eics1080.htm.
[16] IPCS INCHEM, Diethyl carbonate, Int. Programme Chem. Saf. INCHEM, (2000) (Accessed 21 December 2018), http://www.inchem.org/documents/icsc/icsc/eics1080.htm.
[17] Safe and Efficient Hydrocarbon Oxidation Processes by Kinetics and Explosion Expertise, Report on the Experimentally Determined Explosion Limits, Explosion Pressures and Rates of Explosion Pressure Rise – Part1: Methane, Hydrogen and Propylene, (2019) n.d. http://www.morechemistry.com/SAFEKINEX/deliverables/44.Del.%20No.%208.pdf (Accessed 18 March 2018).
[18] A.A. Pekalski, H.P. Schildberg, P.S.D. Smallegange, S.M. Lemkowitz, J.F. Zevenbergen, M. Braithwaite, H.J. Pasman, Determination of the explosion behaviour of methane and propene in air or oxygen at standard and elevated conditions, Process Saf. Environ. Prot. 83 (2005) 421–429, https://doi.org/10.1205/psep.04211.
[19] D. Razus, V. Brinzea, M. Mitu, D. Oancea, Temperature and pressure influence on explosion pressures of closed vessel propane–air deflagrations, J. Hazard. Mater. 174 (2010) 548–555, https://doi.org/10.1016/j.jhazmat.2009.09.086.
[20] D. Razus, V. Brinzea, M. Mitu, C. Movileanu, D. Oancea, Temperature and pressure influence on maximum rates of pressure rise during explosions of propane–air mixtures in a spherical vessel, J. Hazard. Mater. 190 (2011) 891–896, https://doi.org/10.1016/j.jhazmat.2011.04.018.
[21] M. Mitu, V. Giurcan, D. Razus, M. Prodan, D. Oancea, Propagation indices of methane-air explosions in closed vessels, J. Loss Prev. Process Ind. 47 (2017) 110–119, https://doi.org/10.1016/j.jlp.2017.03.001.
[22] A.E. Dahoe, L.P.H. de Goey, On the determination of the laminar burning velocity from closed vessel gas explosions, J. Loss Prev. Process Ind. 16 (2003) 457–478, https://doi.org/10.1016/S0950-4230(03)00073-1.
[23] European standard, EN 1839, Determination of Explosion Limits of Gases and Vapours, (2012).
[24] European standard, EN 13673-1, Determination of the Maximum Explosion Pressure and the Maximum Rate of Pressure Rise of Gases and Vapours - Part 1: Determination of the Maximum Explosion Pressure, (2003).
[25] W.H. Press (Ed.), FORTRAN Numerical Recipes, 2nd ed, Cambridge University Press, Cambridge; New York, 1996.
[26] D.G. Goodwin, H.K. Moffat, R.L. Speth, Cantera: An Object-Oriented Software Toolkit For Chemical Kinetics, Thermodynamics, And Transport Processes. Version 2.3.0, (2017), https://doi.org/10.5281/zenodo.170284.
[27] P.A. Glaude, W.J. Pitz, M.J. Thomson, Chemical kinetic modeling of dimethyl carbonate in an opposed-flow diffusion flame, Proc. Combust. Inst. 30 (2005) 1111–1118, https://doi.org/10.1016/j.proci.2004.08.096.
[28] H. Nakamura, H.J. Curran, A. Polo Córdoba, W.J. Pitz, P. Dagaut, C. Togbé, S.M. Sarathy, M. Mehl, J.R. Agudelo, F. Bustamante, An experimental and modeling study of diethyl carbonate oxidation, Combust. Flame 162 (2015) 1395–1405, https://doi.org/10.1016/j.combustflame.2014.11.002.
[29] G.P. Smith, D.M. Golden, M. Frenklach, N.W. Moriarty, B. Eiteneer, M. Goldenberg, C.T. Bowman, R.K. Hanson, S. Song, W.C.G Jr, V.V. Lissianski, Z. Qin, GRI-MECH 3.0 (n.d.), (2019) (Accessed 18 March 2018), http://www.me.berkeley.edu/gri_mech/.
[30] D. Bradley, T.M. Cresswell, J.S. Puttock, Flame acceleration due to flame-induced instabilities in large-scale explosions, Combust. Flame 124 (2001) 551–559, https://doi.org/10.1016/S0010-2180(00)00208-X.
[31] A.E. Dahoe, Laminar burning velocities of hydrogen–air mixtures from closed vessel gas explosions, J. Loss Prev. Process Ind. 18 (2005) 152–166, https://doi.org/10.1016/j.jlp.2005.03.007.
[32] T. Inoue, K. Mukai, Roles of positive or negative electrodes in the thermal runaway of lithium-ion batteries: accelerating rate calorimetry analyses with an all-inclusive microcell, Electrochem. Commun. 77 (2017) 28–31, https://doi.org/10.1016/j.elecom.2017.02.008.